CIVIL ENGINEERING JOURNAL

Article no. 37

THE CIVIL ENGINEERING JOURNAL 4-2025

PUBLICLY AVAILABLE SPATIAL DATA AS A SOURCE OF COORDINATES FOR GROUND CONTROL POINTS

Jakub Vynikal[1], Jan Pacina[1], Dominik Brétt[1], Jan Popelka[2], Jan Kazan[2] and Jana Müllerová[2]

1. *Department of Geomatics, Faculty of Civil Engineering, Czech Technical University in Prague, Prague, Czech Republic, email: Jakub.vynikal@fsv.cvut.cz*
2. *Department of Geoinformatics, Faculty of Environment, J. E. Purkyně University in Ústí nad Labem, Ústí nad Labem, Czech Republic.*

Received: *13.03.2025*
Received in revised form: *19.06.2025*
Accepted: *02.12.2025*

ABSTRACT

Nowadays, direct georeferencing methods, utilizing GNSS receivers and Inertial Measurement Units (IMUs) on aircraft carriers, are commonly employed to generate products from aerial imagery, including orthophotos and digital elevation models. However, certain scenarios necessitate the utilization of signalized ground control points, such as when higher accuracy is required, large areas need coverage, or GNSS correction data is unavailable. This paper explores leveraging publicly available data, such as orthophotos and digital elevation models, for photogrammetric projects. The methodology involves identifying identical points suitable for embedding from both publicly available data and acquired aerial photographs, retrieving X, Y coordinates from orthophotos, and Z coordinates from elevation (LiDAR) data. Evaluation using advanced geostatistical methods in urban areas and application to landscape documentation in Bohemian Switzerland National Park with diverse photogrammetric sensors demonstrate that the resulting data falls within the accuracy class, meeting standards possibly sufficient even for cadaster needs (based on the national decrees). This approach accelerates photogrammetric imaging preparation and implementation, particularly when aerial vehicles are not equipped with onboard RTK receiver and IMU sensor. Moreover, it contributes to reducing the carbon footprint and environmental impact of aerial imaging by limiting motor vehicle movement within the area of interest to reach, measure and stabilize GCPs.

KEYWORDS

Public data, Orthophoto, LiDAR, Coordinates, Ground control point, Photogrammetry

INTRODUCTION

Nowadays, the use of spatial data derived photogrammetrically from images taken by manned or unmanned systems is a common part of many fields of human activity, in most cases using data in the form of orthophotos or digital models [0]. A critical factor in such derived data is its elevation and positional precision, with different applications requiring different levels of accuracy [0][0][0].

In most cases, imagery acquired by manned or unmanned systems is processed using algorithms based on Structure from Motion modelling [0][0]. In principle, the processing procedure is based on the derivation of a point cloud from the source photographs, which is further used as a

basis for the derivation of a digital surface model and subsequent orthorectification of the aerial photographs [0][0][0].

The quality of the derived photogrammetric model and the subsequent accuracy of the resulting data are influenced by several factors [0][0], with the location of the point cloud in the coordinate system being an important part of the processing (which significantly affects the quality of the result).

There are two basic approaches to georeferencing a photogrammetric model [0] - the first approach is using an unmanned aerial vehicle that has a camera (or other sensor) equipped with an Inertial Measurement Unit (IMU) and a GNSS receiver that allows post-processing with cm accuracy. In this case, the GNSS receiver measures the position of the centre of the image and the IMU unit records the Yaw, Pitch and Roll angles [0]. These data are sufficient to derive a georeferenced point cloud - of course, with an accuracy that matches the accuracy of the IMU and the surveying and post-processing of the GNNS data [0][0][0][17][18].

The second approach uses signalized and geodetically surveyed ground control points (GCP). Many works have been devoted to the issue of the influence of the appropriate number, placement, and accuracy of the GCPs on the quality of the resulting photogrammetric model [19] [20] [21].

The GCPs can also be used in combination with an IMU and a GNSS unit mounted on an unmanned vehicle to increase the accuracy of the derived data (not only for photogrammetry, but also for e.g. laser scanning data) [22] [23] [24].

Usage of affordable spherical photogrammetry is a new trend in heritage documentation, surveying and 3D modeling [25]. Its main advantage is guaranteed overlap and speed of acquisition of a few minutes. The footage doesn't generally reach the quality of pin-hole cameras [26], but it can be used to connect chunks of photos from different places [27]. The presented methodology was tested within the 360° photogrammetry as well.

GCPs can take different forms, in most cases they are either artificially marked (contrasting markers - crosses or squares) or civil infrastructure objects are used like corners of horizontal road markings, corners of pavements, etc. [28] [29] [30]. In practice, suitable positions for the ground control point locations are then identified as part of the development of the survey flight planning. These positions must be usually physically visited, the ground control point marked (target placed), and the coordinates of the ground control point determined using a suitable geodetic method [31] [32].

Nowadays, the widely used is the fast GNSS RTK method, which allows to survey the coordinates of the point with an accuracy of a few centimetres in a matter of seconds, or classical geodesy methods can be used to obtain coordinates with higher accuracy. In remote areas without the presence of stabilised survey points or mobile signal coverage (required for the GNSS RTK method), it is necessary to use GNSS measurement methods using long observations and subsequent post-processing of the data. In addition, it is necessary to remove the marked GCPs once the imaging is completed. All these point embedding activities are thus time consuming and can take several days when imaging remote areas. Not to mention the fact that many areas may be physically inaccessible for direct measurements, e.g. due to terrain geomorphology, strictly protected areas of national parks, or areas affected by natural disasters.

With the increasing digitization of national (geo)data, spatial data in the form of orthophotos and elevation models at the scale of entire countries or large areas are publicly available in many countries [33] [34]. In this paper, we present the possibilities of using naturally signaled GCPs, where their coordinates are read from publicly available and regularly updated data. The X and Y coordinates are read from orthophotos with a spatial resolution of 12.5 cm/pixel, and the Z coordinate is read from airborne laser scanning data with a spatial resolution of 2 m/pixel. Both these data layers are available in Czech Republic (Europe) as Web Map Services (WMS) and "open data". The aim of our research is to verify the accuracy of the data (both orthophoto and elevation model) derived by photogrammetric methods without direct field measurements. This approach significantly streamlines the aerial imagery preparation process, reduces the cost of the entire imagery process, and ultimately reduces the carbon footprint.

The test data set was created in a built-up area, where a network of GCPs and check points was surveyed by GNSS RTK. The accuracy of the resulting photogrammetric model was evaluated using advanced geostatistical methods. Then, this approach was implemented in the Bohemian Switzerland National Park (NP, Czech Republic), where two surveys were conducted, RGB photogrammetric imaging in September 2022, and multispectral imaging in May 2023. Within this NP, large areas are inaccessible due to the geomorphology of the terrain (sandstone cliffs), the protection of fauna and flora, a large wildfire in 2022 and the ongoing bark beetle calamity. Obtaining the coordinates of the GCPs from publicly available data is thus an optimal way to georeference the photogrammetric models in such area with sufficient accuracy. We also applied the same strategy on a small-scale project, a photogrammetric survey of a small modernist building and its surroundings, using UAV and terrestrial photogrammetry including the spherical one.

MATHERIALS AND METHODS

The overall methodology is described as follows. The main objective was to assess the accuracy of photogrammetric outputs georeferenced using coordinates derived from publicly available spatial data (orthophoto and elevation model), as an alternative to ground-surveyed GCPs. The workflow consists of the following steps:

1.) Selection of test areas — Three types of test cases were used:
   a) Urban area (Ústí nad Labem)
   b) Natural protected area (Bohemian Switzerland NP, wildfire and multispectral datasets)
   c) Small-scale urban object (building)

2.) Acquisition of aerial imagery — Using UAVs or aircraft, in RGB or multispectral modes, or 360° photography.

3.) Ground truth survey — Collection of GCP and check point coordinates using RTK GNSS and total station, for reference evaluation.

4.) Reading of public data coordinates — Extraction of X, Y coordinates from orthophoto (CUZK) and Z coordinates from national LiDAR model (DMR5G), to serve as public data GCPs.

5.) Photogrammetric processing — Processing of imagery in Agisoft Metashape, using both:
   a) Ground-surveyed (GNSS) GCPs and CPs
   b) Public-data-based (CUZK) GCPs and CPs - following the same photogrammetric parameters and workflow.

6.) Statistical evaluation — For each dataset, model errors (differences between photogrammetric output coordinates and ground truth) were analyzed:
   a) Spatial autocorrelation — Global Moran's I
   b) Normality and central tendency — Jarque-Bera, Doornik-Hansen, t-test, Wilcoxon
   c) Elevation dependence — Spearman's rho, least trimmed squares (LTS) regression
   d) Comparison of CUZK vs. GNSS models (variance, bias).

This workflow enables comparison of the photogrammetric accuracy achievable using public spatial data against the traditional GNSS-based approach, across different types of environments and data qualities.

PUBLICLY AVAILABLE DATA

In the Czech Republic, photogrammetric imaging has been carried out since the 1920s. Currently, a wide range of spatial data is available for the territory - in addition, from 1 July 2023, national maps, orthophotos and an elevation model (derived from aerial LiDAR data) are available as open-data [35]. For the methodology presented in this paper, two of the datasets are relevant - Orthophoto of the Czech Republic (used here to derive X, Y coordinates) and Digital Terrain Model

of the Czech Republic of the 5th generation (used here to derive Z coordinate). Both of these datasets are provided by the Czech Office for Surveying, Mapping and Cadastre.

During the past 20 years of development and production of the Orthophoto of the Czech Republic, in which the Ministry of Defence, the Ministry of Agriculture and the Czech Office for Surveying, Mapping and Cadastre participate, several major measures have been taken: in 2009, the original ground sampling distance (GSD) was increased from 0.50 m to 0.25 m. Since 2010, digital aerial survey cameras have been used exclusively. In 2012, the original orthophoto update period was reduced from three to two years. In 2016-2017, the GSD was further increased to 0.20 m, that was further increased to 0.125 m in 2021. The quality of the processed CR orthophoto for the 2021 data within the area relevant to our research (western part of the Czech Republic) was an overall characteristic mean positional error of 0.233 m and the corresponding mean coordinate error of 0.165 m for well identified but artificially unsignalized objects [36].

The Digital Model of Relief of the Czech Republic, 5th generation (DMR 5G) represents a digital representation of land surface in the form of heights of discrete points in an irregular triangular network (TIN) of points with coordinates X,Y,H, where H represents the altitude in the Baltic height reference system after levelling (Bpv) with a total mean height error of 0.18 m in exposed terrain, and 0.3 m in forested terrain. The model was created from data acquired by the method of airborne laser scanning in 2009 - 2013 [35].

AREAS OF INTEREST AND DATA COLLECTION

Quality verification of X, Y and Z coordinate readings from publicly available spatial data sources in the city centre of Ústí nad Labem (Czech Republic).

The SONY ILCE-6000 camera model in combination with a 16 mm focal length lens (Sony 16 mm f/2.8 SEL) was used to take a total of 2353 images of the city centre with a final resolution of 6000 x 4000 pixels, i.e. 24 Mpx and a pixel size of 4 x 4 μm. The mapped area of 3 km^2 was photographed from a height of approx. 300 m, resulting in an average GSD of 7 cm. The overlap of the images was uneven due to the nature of the flight, but it was sufficient, about 80%.

In order to reference the photogrammetric model to the coordinate system, it was necessary to locate the GCPs. In addition, check points were acquired to independently verify the resulting quality of the derived data. For this purpose, we used a GNSS receiver with RTK type HIPER SR from TOPCON, which employs GPS and GLONASS satellites for position recording. To ensure centimeter level accuracy of the measurements, we used the RTK method using the national network of permanent stations CZEPOS. The points had to be selected based on their visibility in public orthophoto. This task was much more challenging in the rural forested area, where clearly signalized objects on the terrain were only sparse due to lack of man-made clearly defined structures. Nevertheless, a sufficient number of points was identified.

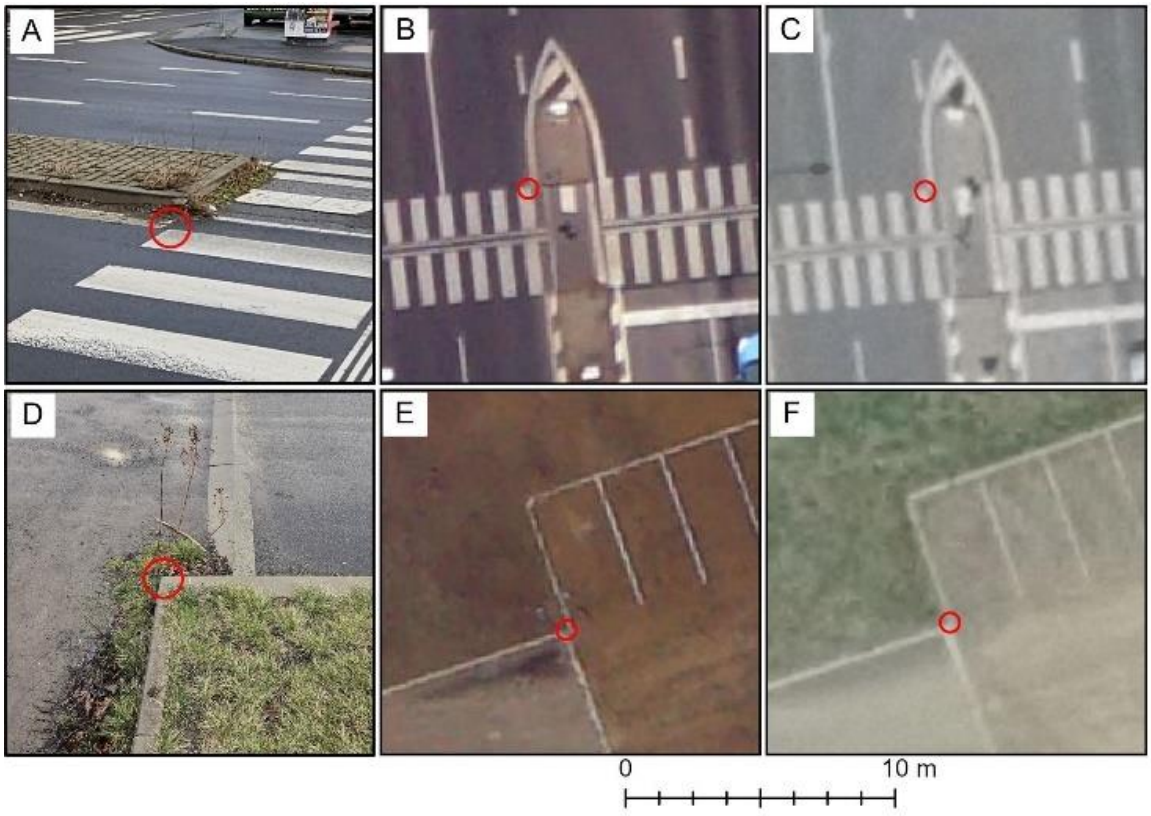

Fig. 1 - Example of ground control point selection within the test dataset. A, D - point in reality; B,E - point in acquired aerial image; C, F - point in publicly available orthophoto

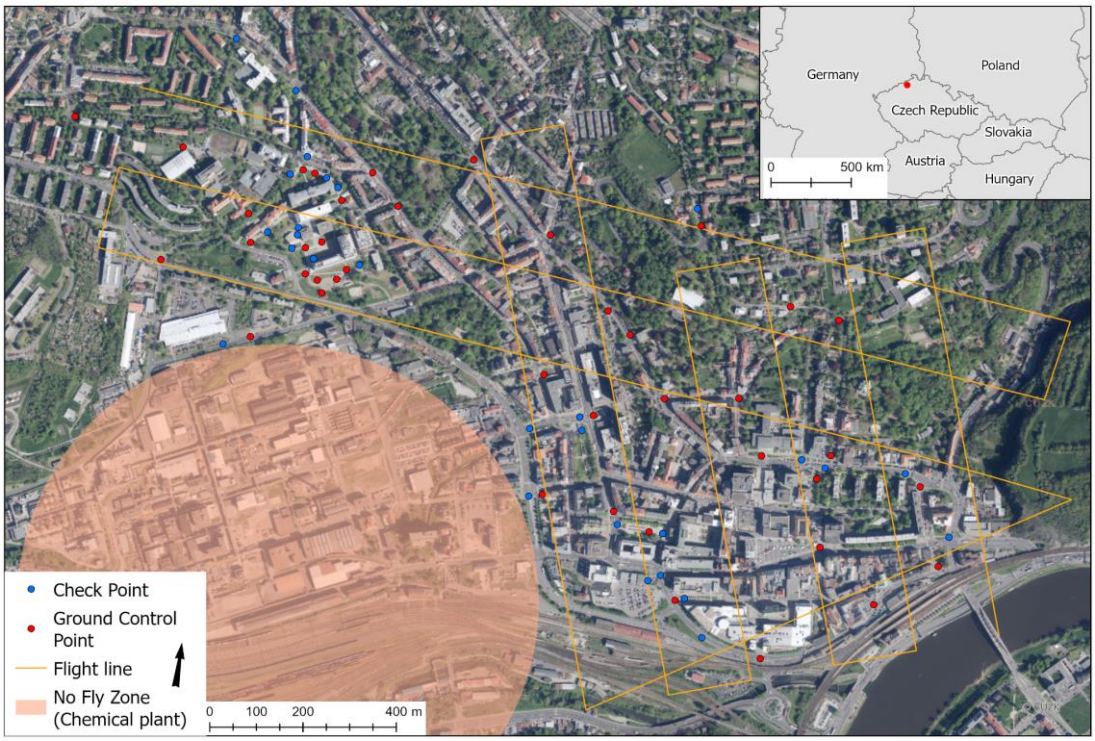

Fig. 2 - Ground control point and check point distribution within the area of interest

The measurements were repeated with time intervals and the values of the measured coordinates were averaged. The points were evenly distributed in the test area in the number of 41

and horizontal traffic signs, corners of pavements and stairs were chosen to signal these points (see Figure 1 and Figure 2). The X, Y and Z coordinates of all GCPs were also read from publicly available orthophoto and LiDAR data (CUZK model).

The methodology of reading the coordinates of GCPs using publicly available data has been practically applied in the area of the NP. The area of this NP is a good example of benefits of this indirect readout of GCPs, as a large part of the NP is inaccessible due to its geomorphology (rugged sandstone cliffs and canyons) and strict nature protection.

In addition, in August 2022, a significant part of the NP (more than 10 km^2 out of a total area of 80 km^2) was affected by a forest fire (the largest in the history of the NP and the Czech Republic). During the firefighting and subsequent damage surveys, it was not possible to take imagery of the affected area using unmanned aerial vehicles, nor to signal/measure GCPs in the affected area (see Figure 3).

Fig. 3 - Wildfire site and the inaccessible terrain within the Bohemian Switzerland national park. Photo from September 2022

Thus, a small aircraft equipped with a Hasselblad A6D-100 camera with HS 3.5/50mm-II lens was used to document the situation just after the wildfire. Imaging was carried out in early September 2022 from an altitude of 600 m. A total of 1920 images were taken. 10 GCPs were used for processing (see Figure 4). The spatial resolution of processed orthophoto is 5 cm/pixel.

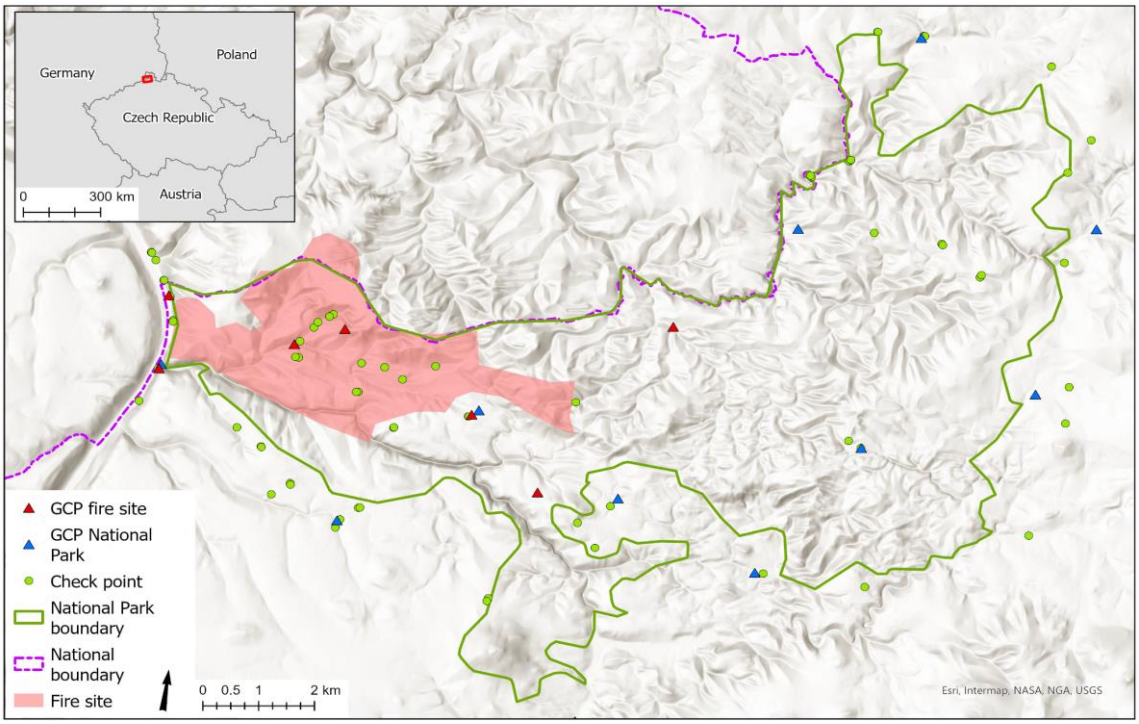

Fig. 4 - Area of interest within the Bohemian Switzerland national park. Distribution of ground control points, check points, wildfire site and multispectral imagery coverage

Additional aerial photography was conducted in late May 2023, aimed at assessing vegetation status throughout the NP (including the wildfire area). For this imagery, the Micasense Altum multispectral camera was used, allowing imaging in 6 bands. Imagery was taken from the same small aircraft in altitude of 600 m. In total, about 6000 six-band images were taken. For processing, 10 GCPs were defined (see). The spatial resolution of processed orthophoto is 35 cm/pixel.

During July 2023, a total of 71 check points were surveyed in the whole NP area to verify the quality of the processed data, thereof 69 of measured points were acquired with RTK method and 2 points with fast static method due to lack of mobile network connection (see Figure 4).

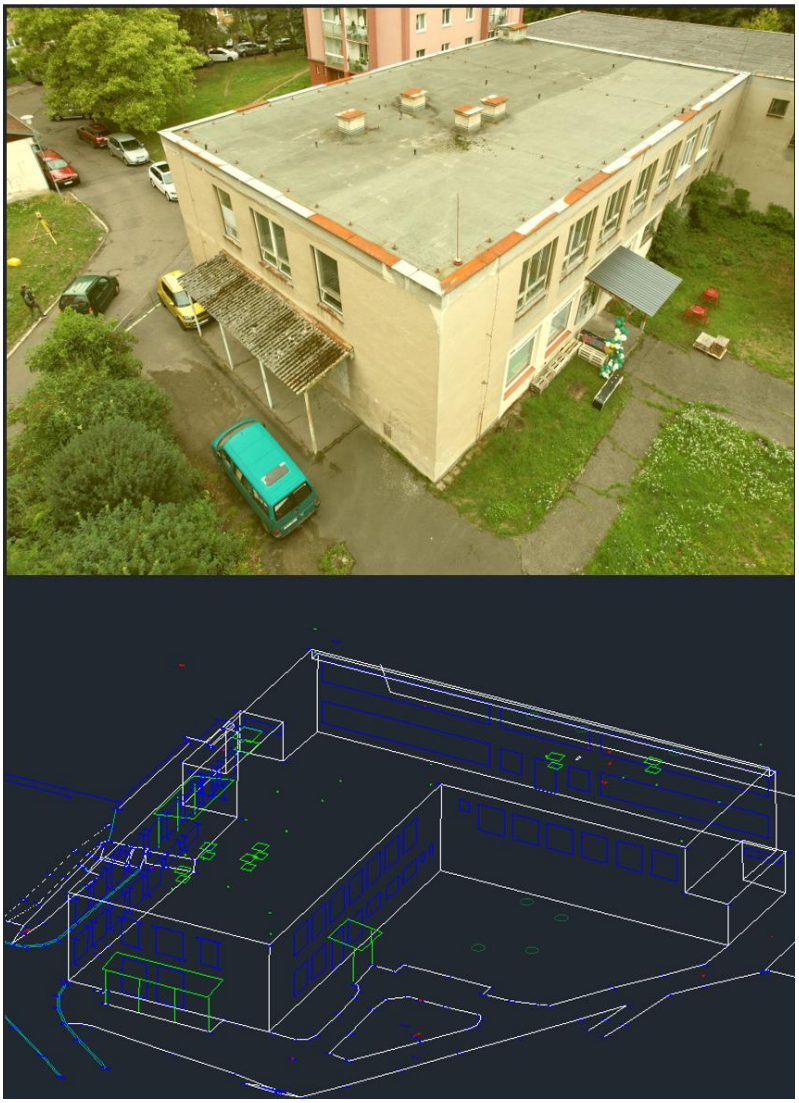

Fig. 3 - Structure modelled using the UAV and 360° photogrammetry

Lastly, we test the proposed method on a small-scale photogrammetry project, concerning documentation of a two-story building using terrestrial and UAV photogrammetry (see Figure 5). For this small photogrammetry project, we chose a modernist structure in a town with a sufficient amount of naturally signalized control points nearby. Part of documentation was conducted using conventional methods with total station and GNSS rover, including stabilization of precise control points. This was followed with UAV and 360° photogrammetry. The UAV utilized was DJI Air 2S, with 1-inch 20 MPix sensor. Height of the flight was around 20 meters, both grid and oblique. Data collection using the drone was carried out according to the legislation in force.

The 360° footage was obtained using Insta360 RS 1-inch camera, mounted on a telescopic pole. Three walkarounds with variable instrument height were conducted. The camera recorded video at 6K resolution, which was later sampled every 1 meter to 17 MPix frames. Overall, 138 aerial photos and 642 spherical frames were acquired.

PHOTOGRAMMETRIC PROCESSING

Aerial photos covering the test area in Ústí nad Labem were imported to industry standard software Agisoft Metashape, version 1.8.3 (build 14298). The alignment step was performed on 'High' accuracy with standard setting of 40,000 key point limit and 4,000 tie point limit. After importing coordinates of GCPs and CPs, all naturally signalized points were marked on a sufficient number of

photos. The alignment was then optimized with all interior parameters fitted, along with the 'Fit additional corrections' option checked. This option allows for estimation of additional parameters, in case of datasets with strong geometry and sufficiently overdetermined bundle adjustment, resulting in potentially better alignment [37]. This was confirmed with residuals on check points being slightly lower than without additional corrections. The prior marker accuracy was set to 10 cm, as such value represents expected accuracy of the public orthophoto and terrain model. As the naturally signalized points are not usually as precisely identifiable as dedicated black and white targets, we lowered the expected accuracy of their image coordinates to 1 pixel. The camera was not pre-calibrated, but in case of non-metric cameras, it is not a necessity, since it is usually sufficient to perform the calibration within the bundle adjustment [38].

Multispectral images were also processed in Agisoft Metashape, version 1.8.4 (build 14856). The processing parameters used were the same as for the test dataset, except that the multispectral data processing methodology (including reflectance calibration) was applied to the data.

The processing of the small-scale urban dataset took place once again in Agisoft Metashape, with similar parameters as in the test dataset. Spherical video was stitched in Insta360 software in post-processing to a full equirectangular panorama. For the 360 footage to align properly, it is necessary to set the camera type in Metashape to 'spherical'.

STATISTICAL METHODS

The evaluation and testing of three key quality criteria related to model errors (differences between model and real coordinates) were conducted [39][40]. These criteria are as follows:

1. Model errors should not exhibit spatial autocorrelation; instead, they should be randomly distributed in space. To assess this, the global Moran's index was employed, with significance determined using the P-value from the normally distributed z-score. The Spatial Autocorrelation (Global Moran's I) tool in ArcGIS Pro (version 3.2.0) was used for these calculations.

2. Errors should follow a normal (or at least symmetric) distribution with a mean value of zero. The Jarque-Bera test was applied for univariate normality assessment, while the Doornik-Hansen test evaluated multivariate normality—both tests rely on skewness and kurtosis measures. Measures of central tendency were tested using a univariate test for equality to zero (t-test for sample mean, Wilcoxon test for sample median). All measures and tests, as well as standard deviation, standardized skewness, standardized kurtosis and box plots were computed using the PAST (ver. 4.16c) software. PAST also facilitated two-sample paired t-tests for means, Wilcoxon tests for medians, and F-tests for variances, all of which were used to compare CUZK and GNSS model errors.

3. Model errors should not be dependent on elevation, meaning there should be neither linear nor monotonic correlation. Spearman's rank correlation coefficient was used to evaluate this relationship, as it is robust against outliers and easy to test for significance. Linear regression was employed to further investigate dependencies between model errors and elevation. However, since outliers can significantly bias ordinary least squares (OLS) regression estimates [41], least trimmed squares (LTS) regression was used as a more robust alternative. Unlike OLS, LTS regression minimizes the impact of outliers, providing more reliable parameter estimates. Correlation analysis and LTS regression were conducted using PAST software (version 4.16c). While parametric error estimates are not available for LTS regression, PAST provides 95% bootstrapped confidence intervals for both slope and intercept.

RESULTS

URBAN DATASET

In the data processing, we focused on the following procedure: To rigorously test the proposed methodology, the area of the city of Ústí nad Labem was photogrammetrically processed

using the coordinates of the GCPs obtained both by direct measurement (GNSS model) and subtracted from publicly available spatial data (CUZK model). Advanced geostatistical techniques were used to analyze the resulting differences in X, Y and Z coordinates. Based on the results obtained, the three main quality criteria of the model errors (spatial autocorrelation, normal distribution and elevation stability, presented in section Statistical methods), the GNSS model met the defined criteria, while the CUZK model did not meet the normality condition.

*Tab. 1 - Descriptive statistics, Rank correlation coefficients, Normality tests and Global Moran's Indexes of model errors for CUZK and GNSS model. Statistical significance if tested: † not significant, * p-value <0.1, ** p-value <0.05, *** p-value < 0.01. 95% bootstrapped confidence intervals (N=1999)*

Method	CUZK			GNSS		
	X	Y	Z	X	Y	Z
Spatial autocorrelation (Moran's Index)	-0.099†	-0.074†	0.098†	-0.099†	-0.074†	0.098†
Mean	-0.001†	0.003†	0.052***	-0.002†	0.009†	-0.006†
Median	-0.010†	-0.001†	0.044**	0.005†	0.002†	-0.006†
Standard Deviation	0.063	0.072	0.155	0.050	0.059	0.103
Standardized Skewness	0.651	0.090	0.025	0.288	0.434	-0.386
Standardized Kurtosis	0.415	-0.546	-0.129	-0.444	0.139	0.689
Normality (Jarque-Bera JB)	4.996*	1.114†	0.129†	1.650†	2.108†	2.561†
Multivariate normality (Doornik and Hansen omnibus)	6.111†			7.405†		
Spearman Rank Correlation	-0.007†	0.169†	0.174†	0.087†	0.222*	0.227*
LTS regression - bootstrapped 95% confidence intervals on slope	(-0.003, 0.001)	(-0.005, 0.001)	(-0,002, 0.006)	(-0.001, 0.003)	(-0.001, 0.003)	(-0.006, 0.001)

As presented in Table 1, Moran's indices were not statistically significantly different from zero, i.e. the errors of both models were not spatially clustered and were randomly distributed. The second criterion tested, the normality of the error distribution, was measured using skewness and kurtosis

statistics (see Table 1) and tested by Jarque-Bera (univariate normality) and the powerful omnibus (overall) test due to Doornik & Hansen (multivariate normality).

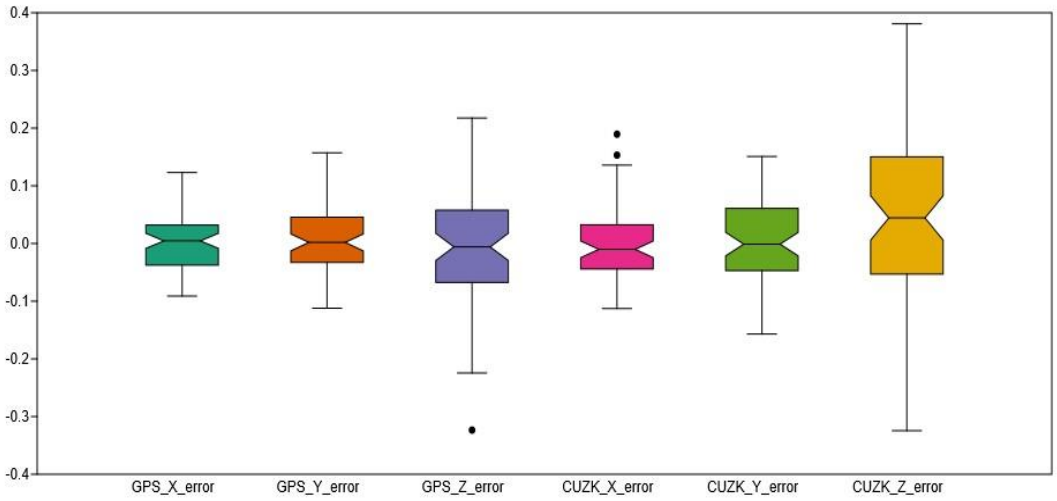

Fig. 4 - Boxplots of errors with outliers and notches denoting

The normality tests, as well as the skewness and kurtosis statistics, show that only the X errors of the CUZK model are non-symmetrically distributed. The skewness of the errors is positive, negative errors predominate and outliers are present (see Figure 6). The Z errors of the CUZK model violate the second rule in a different way: although they are normally distributed, the measures of central tendency (both mean and median) are statistically significantly greater than 0 (see Table 1 and Figure 6). According to the 95% confidence interval, the mean error is between 1.5 and 8.9 cm.

The elevation stability (error as a monotonic function of elevation) was assessed using Spearman's rank correlation coefficients. The results (see Table 1) show that the Y and Z errors of the GNSS model are positively correlated with elevation. However, the correlation is weak. Looking closely at the slope estimates obtained by the robust Least trimmed square regression (LTS), or more precisely at the 95% bootstrapped confidence intervals, makes it clear that the errors are not elevation depended as all intervals contain the 0 value. We can thus conclude that the estimated slopes are not statistically significant.

The comparison of the measures of central tendency (both mean and median) and variance shows bias of the CUZK Z errors, and a significantly higher variability of the X, Y and Z errors of the CUZK model (see Table 2)

*Tab. 2 - Differences between GNSS and CUZK models and tests of their statistical significance. Statistical significance: * p-value <0.1, ** p-value <0.05, *** p-value < 0.01*

Test \ Coordinate	X	Y	Z
Differences of means (t-test)	0.001	0.005	0.058***
Differences of medians (Wilcoxon test)	0.015	0.003	-0.050***
Ratio of variances (F-test)	1.633*	1.508*	2.263***

This validated methodology was applied to three different datasets - a wildfire site in the NP (detailed data obtained from RGB imagery), the entire NP (multispectral data of low spatial resolution, Figure 4), and detailed building modelling within urban area.

The acquired aerial photographs were photogrammetrically processed into orthophotos and digital surface models. Suitable check points were then identified in the GIS environment, and subsequently surveyed in the field using the GNSS method (noted as GNSS in the on following Tabs). The distribution of these points is shown in Figure 4. The X and Y coordinates of the identified check points were derived from the produced orthophoto and Z coordinates from the digital surface model (noted as Model in the on following Tabs). Subsequently, the differences between these coordinates (GNSS - Model) were compared. Table 3 provides an assessment of the accuracy of the urban dataset that was subjected to the robust statistical evaluation in this section in order to compare the results with the other processed datasets.

Tab. 3 - Comparison of points from bundle alignment and control points - urban dataset. Error values in cm

Model - GNSS	N°	Y (cm)	X (cm)	Z (cm)	XY (cm)	XYZ (cm)
GCPs RMSE	41	7.1	7.7	14.7	10.5	18.1
CPs sys. err.	29	0.3	-0.9	12.6	0.9	12.6
CPs rand. err.	29	4.9	6.3	13.2	7.9	15.4
CPs RMSE	29	4.9	6.3	18.2	8.0	19.9

NATIONAL PARK WILDFIRE SITE

RGB images (acquired with the Hasselblad A6D-100 camera) were overlaid on 10 points subtracted from a combination of orthophoto and LiDAR data (Model). Due to the nature of the terrain, finding identifiable points was more difficult than in the case of the city center above. A similar procedure to the validated urban dataset was used to calculate the bundle alignment and derived photogrammetric products. The results of the comparison between the model coordinates and the coordinates acquired by GNSS are presented in Table 4. Within this area, 24 control points were used for quality verification. An example of the identifiability of selected control points is shown in Figure 7 - C.

Tab. 4 - Comparison of points from bundle alignment and control points – wildfire site. Error values in cm

Model - GNSS	N°	Y (cm)	X (cm)	Z (cm)	XY (cm)	XYZ (cm)
GCPs RMSE	10	6.8	14.6	24.1	16.2	29.0
CPs sys. err.	24	-1.3	8.9	13.6	9.0	16.3
CPs rand. err.	24	15.0	10.0	36.6	18.0	40.8
CPs RMSE	24	15.1	13.3	39.0	20.1	43.9

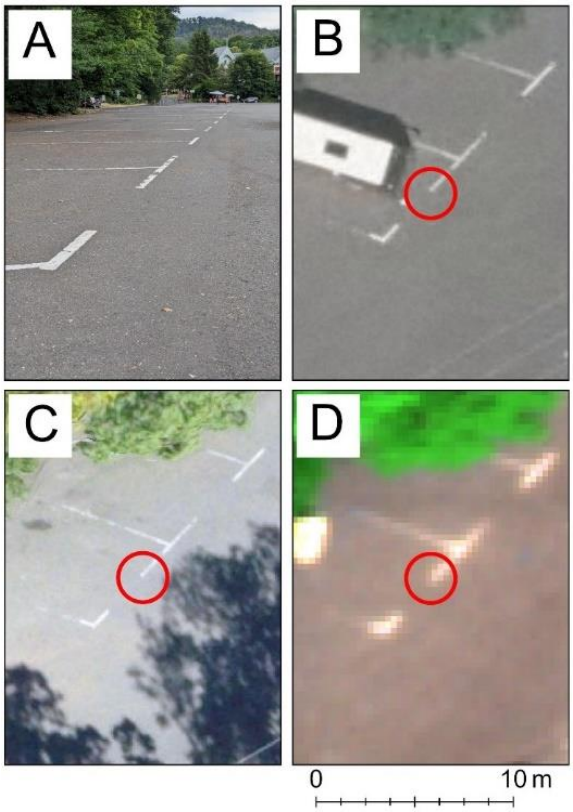

Fig. 5 - Example of check point measured within the Bohemian Switzerland national park. A – reality; B – publicly available orthophoto; C – Hasselblad A6D-100 aerial image; D – Micasense Altum aerial image

NATIONAL PARK MULTISPECTRAL DATASET

In this case, the multispectral data was acquired (using the Micasense Altum camera) for the whole area of the NP. Finding identifiable points was difficult as the resolution of the images corresponds to approximately 30 cm. The 10 GCPs from the public data and 67 control points located by GNSS were used. The resulting quality assessment is shown in Table 5. An example of the identifiability of selected control points is shown in Figure 7 - D.

Tab. 5 - Comparison of points from bundle alignment and control points – multispectral dataset. Error values in cm

Model - GNSS	N°	Y (cm)	X (cm)	Z (cm)	XY (cm)	XYZ (cm)
GCPs RMSE	10	41.6	29.5	95.9	51.0	108.7
CPs sys. err.	67	-26.9	-1.7	71.2	26.9	76.1
CPs rand. err.	67	84.2	49.4	588.5	97.6	596.6
CPs RMSE	67	88.4	49.4	592.8	101.2	601.4

SMALL SCALE DATASET

In this case, a model of the building and its surroundings was created using drone imagery and spherical photography. For the documentation purposes, a CAD drawing was created, along

with orthomosaics. The quality of the resulting model was verified using 12 control points. Due to the nature of the data, the RMSE at each insertion point was not evaluated (see Table 6).

Tab. 6 - Comparison of points from bundle alignment and control points – small scale dataset. Error values in cm

Model - GNSS	X (cm)	Y (cm)	Z (cm)	XY (cm)	XYZ (cm)
CPs sys. err.	2.3	-9.8	-7.6	10.1	12.6
CPs rand. err.	7.0	7.8	7.4	10.5	12.9
CPs RMSE	7.4	12.5	10.6	14.6	18.0

CONCLUSION

The aim of the presented research was to verify the possibilities of using publicly available spatial data, such as orthophotos and digital elevation models, for aerial image embedding. This approach can be specifically useful in cases where the photogrammetric data collection equipment (aircraft, drone) is not equipped with an IMU unit, or where the IMU unit records data with insufficient accuracy, and at the same time it is problematic or time and economically unprofitable to deploy and signal the GCPs.

The quality of this procedure was verified by advanced statistical analysis of a photogrammetrically acquired dataset, which was fully covered by a large dataset of both GCPs and check points. As part of the testing, the coordinates of these points were both located using the GNSS method and read from publicly available data - X and Y coordinates from national orthophoto collection and Z coordinates from nation-wide LiDAR dataset.

The resulting accuracy was evaluated according to three criteria that have been proven in the past to be suitable for comprehensive evaluation of spatial data accuracy – it is expected random distribution of errors in space, errors with normal distribution and mean equal to 0, and the resulting model being elevationally stable. The tested data (derived from publicly available national dataset) meet all specified quality criteria, except for the Z coordinate which violates the second criterion with a mean height error statistically different from zero and a confidence interval for the mean between 1.5 and 8.9 cm. This is explained by the fact that the publicly available Lidar data for the Czech Republic shows, despite stated full mean error of height in open terrain of 18 cm, systematic overestimation by up to 10 cm.

Thus, our results proved that the method of embedding using publicly available data is applicable in practice, and its accuracy, in the case of our detailed dataset, satisfies the quality of points of accuracy class 3, which is defined by the mean coordinate error of the detailed point of the position map m_{xy} = 0.14 meters. This accuracy is currently satisfactory for land registry purposes in the Czech Republic.

To proof the concept, the tested method was then applied to the RGB dataset (GSD 5 cm) in the sandstone area of the Bohemian Switzerland NP. The search for identifiable points was more difficult here, however, the accuracy achieved in Table 4 is still very high. According to the annex of the cadastral decree, in a dataset containing more than 20 points, at least 40% of the sampling mean coordinate errors must be smaller than the value of the basic mean coordinate error (Decree No. 357/2013 Coll. on the Czech Land Registry). In our case, this condition is met by 15 out of 24 points, i.e. 62.5%. Only one point just exceeded the coordinate error threshold. The cumulative sampling mean coordinate error reached 14.2 cm, which, when rounded, is just the characteristic of quality code 3 (note: we consider GNSS points as fixed).

This method was also applied to the multispectral dataset of coarser GSD of 35 cm spanning larger area of the whole NP. For this dataset, significant accuracy margins were evident, mainly due to the lack of GCPs. In one area without tie points, the error in the height coordinate was over 10 m.

The mean plane position error was around 1 m, which is sufficient for many environmental purposes. The mean elevation error was much larger and more GCPs would be needed to reduce it.

Finally, the tested method was applied to a dataset that is defined on a small scale (building). With respect to the high precision data collection methods, the resulting quality assessment scores correspond to quality point code 3.

To summarize, when selecting GCPs from publicly available data, it is advisable to apply the same philosophy as when signalling GCPs in the field - points evenly distributed within the area that are clearly identifiable. Furthermore, it has proven to be appropriate to select points that are located on a plane (or have a flat surroundings), as the reference digital elevation model might not respect (with respect to point density, subsequent interpolation) the dynamic changes of the relief. This implies another condition - namely the actual quality of the reference dataset, which should be defined or verified in the field.

The presented method of ground control point selection based on publicly available data represents a way to efficiently photogrammetrically process large areas while minimizing time and financial costs, and also considering the reduction of the carbon footprint associated with the use of motorized vehicles during GCPs measurements.

ACKNOWLEDGEMENTS

This research was funded by Student Grant Competition of Czech Technical University in Prague, grant SGS25/046/OHK1/1T/11 (JV), and by Technology Agency of the Czech Republic, project SS05010090 (all authors).

REFERENCES

[1] Lamsters K, Karušs J, Krievāns M, Ješkins J (2020) High-resolution orthophoto map and Digital Surface models of the largest Argentine Islands (the Antarctic) from Unmanned Aerial Vehicle photogrammetry. Journal of Maps 16:335–347. doi: 10.1080/17445647.2020.1748130

[2] Biyik MA, Atik ME, Duran Z (2023) Deep learning-based vehicle detection from orthophoto and spatial accuracy analysis. International Journal of Engineering and Geosciences 8:138–145. doi: 10.26833/ijeg.1080624

[3] Boon MA, Tesfamichael S (2017) Wetland vegetation integrity assessment with low altitude multispectral UAV imagery. The International Archives of the Photogrammetry, Remote Sensing and Spatial Information Sciences XLII-2/W6:55–62. doi: 10.5194/isprs-archives-xlii-2-w6-55-2017

[4] Güngör R, Uzar M, Atak B, et al (2022) Orthophoto production and Accuracy Analysis with UAV photogrammetry. Mersin Photogrammetry Journal 4:1–6. doi: 10.53093/mephoj.1122615

[5] Ullman S (1979) The interpretation of structure from motion. Proceedings of the Royal Society of London, B203.

[6] Seitz SM, Curless B, Diebel J, et al A comparison and evaluation of Multi-View Stereo Reconstruction Algorithms. 2006 IEEE Computer Society Conference on Computer Vision and Pattern Recognition - Volume 1 (CVPR'06). doi: 10.1109/cvpr.2006.19

[7] Brutto ML, Meli P (2012) Computer vision tools for 3D Modelling in archaeology. International Journal of Heritage in the Digital Era 1:1–6. doi: 10.1260/2047-4970.1.0.1

[8] Verhoeven G (2011) Taking computer vision aloft – archaeological three-dimensional reconstructions from aerial photographs with Photoscan. Archaeological Prospection 18:67–73. doi: 10.1002/arp.399

[9] Verhoeven G, Doneus M, Briese Ch, Vermeulen F (2012) Mapping by matching: A computer vision-based approach to fast and accurate georeferencing of archaeological aerial photographs. Journal of Archaeological Science 39:2060–2070. doi: 10.1016/j.jas.2012.02.022

[10] Ludwig M, M. Runge C, Friess N, et al (2020) Quality Assessment of photogrammetric methods—a workflow for reproducible UAS ORTHOMOSAICS. Remote Sensing 12:3831. doi: 10.3390/rs12223831

[11] Taddia Y, González-García L, Zambello E, Pellegrinelli A (2020) Quality Assessment of photogrammetric models for façade and building reconstruction using DJI Phantom 4 RTK. Remote Sensing 12:3144. doi: 10.3390/rs12193144

[12] Štroner M, Urban R, Seidl J, et al (2021) Photogrammetry using UAV-mounted GNSS RTK: Georeferencing Strategies without GCPS. Remote Sensing 13:1336. doi: 10.3390/rs13071336

[13] Rizaldy A, Firdaus W (2012) Direct georeferencing : A new standard in photogrammetry for high accuracy mapping. The International Archives of the Photogrammetry, Remote Sensing and Spatial Information Sciences XXXIX-B1:5–9. doi: 10.5194/isprsarchives-xxxix-b1-5-2012
[14] Brodie MA, Walmsley A, Page W (2008) The static accuracy and calibration of inertial measurement units for 3D orientation. Computer Methods in Biomechanics and Biomedical Engineering 11:641–648. doi: 10.1080/10255840802326736
[15] Dinkov D (2023) Accuracy assessment of high-resolution terrain data produced from UAV images georeferenced with on-board PPK positioning. Journal of the Bulgarian Geographical Society 48:43–53. doi: 10.3897/jbgs.e89878
[16] Vieira D, Orjuela R, Spisser M, Basset M (2022) Positioning and attitude determination for precision agriculture robots based on IMU and two RTK gpss sensor fusion. IFAC-PapersOnLine 55:60–65. doi: 10.1016/j.ifacol.2022.11.115
[17] Pavelka, K., Raeva, P. and Pavelka, K. (2022) 'Evaluating the performance of airborne and ground sensors for applications in precision agriculture: Enhancing the postprocessing state-of-the-art algorithm', Sensors, 22(19), p. 7693. doi:10.3390/s22197693.
[18] Pavelka, K., Šedina, J. and Pavelka, K. (2021) 'Knud Rasmussen Glacier Status Analysis based on historical data and moving detection using RPAS', Applied Sciences, 11(2), p. 754. doi:10.3390/app11020754.
[19] Nagendran SK, Tung WY, Mohamad Ismail MA (2018) Accuracy assessment on low altitude UAV-borne photogrammetry outputs influenced by ground control point at different altitude. IOP Conference Series: Earth and Environmental Science 169:012031. doi: 10.1088/1755-1315/169/1/012031
[20] Tahar KN (2013) An evaluation on different number of ground control points in unmanned aerial vehicle photogrammetric block. The International Archives of the Photogrammetry, Remote Sensing and Spatial Information Sciences XL-2/W2:93–98. doi: 10.5194/isprsarchives-xl-2-w2-93-2013
[21] Ulvi A (2021) The effect of the distribution and numbers of ground control points on the precision of producing orthophoto maps with an unmanned aerial vehicle. Journal of Asian Architecture and Building Engineering 20:806–817. doi: 10.1080/13467581.2021.1973479
[22] Ilci V, Toth C (2020) High definition 3D map creation using GNSS/IMU/LIDAR sensor integration to support Autonomous Vehicle Navigation. Sensors 20:899. doi: 10.3390/s20030899
[23] Běloch, L. (2025) 'Impact of terrain and environment on the accuracy of vehicle-based Mobile Mapping Systems', Stavební obzor - Civil Engineering Journal, 34(2), pp. 291–303. doi:10.14311/cej.2025.02.0020.
[24] Běloch, L. and Pavelka, K. (2024) 'Optimizing Mobile Laser scanning accuracy for urban applications: A comparison by strategy of different measured ground points', Applied Sciences, 14(8), p. 3387. doi:10.3390/app14083387.
[25] Barazzetti L, Previtali M, Roncoroni F (2022) 3D modeling with 5K 360° videos. The International Archives of the Photogrammetry, Remote Sensing and Spatial Information Sciences XLVI-2/W1-2022:65–71. doi: 10.5194/isprs-archives-xlvi-2-w1-2022-65-2022
[26] Reznicek, J. (2014) 'Method for measuring lens distortion by using Pinhole Lens', The International Archives of the Photogrammetry, Remote Sensing and Spatial Information Sciences, XL–5, pp. 509–515. doi:10.5194/isprsarchives-xl-5-509-2014.
[27] Barazzetti L, Previtali M, Roncoroni F, Valente R (2019) Connecting inside and outside through 360° imagery for close-range photogrammetry. The International Archives of the Photogrammetry, Remote Sensing and Spatial Information Sciences XLII-2/W9:87–92. doi: 10.5194/isprs-archives-xlii-2-w9-87-2019
[28] McMahon C, Mora OE, Starek MJ (2021) Evaluating the performance of SUAS photogrammetry with PPK positioning for infrastructure mapping. Drones 5:50. doi: 10.3390/drones5020050
[29] Oniga V-E, Breaban A-I, Statescu F (2018) Determining the optimum number of ground control points for obtaining high precision results based on UAS Images. The 2nd International Electronic Conference on Remote Sensing. doi: 10.3390/ecrs-2-05165
[30] Rabins LF, Theuerkauf EJ, Bunting EL (2023) Using existing infrastructure as ground control points to support citizen science coastal UAS Monitoring Programs. Frontiers in Environmental Science. doi: 10.3389/fenvs.2023.1101458
[31] Martínez-Carricondo P, Agüera-Vega F, Carvajal-Ramírez F, et al (2018) Assessment of UAV-photogrammetric mapping accuracy based on variation of Ground Control Points. International Journal of Applied Earth Observation and Geoinformation 72:1–10. doi: 10.1016/j.jag.2018.05.015
[32] Tomaštík J, Mokroš M, Surový P, et al (2019) UAV RTK/PPK method—an optimal solution for mapping inaccessible forested areas? Remote Sensing 11:721. doi: 10.3390/rs11060721
[33] European data. The official portal for European data. https://data.europa.eu/en. Accessed 11 Mar 2024
[34] USGS. EarthExplorer. https://earthexplorer.usgs.gov/. Accessed 11 Mar 2024
[35] ČÚZK. Open data of the Czech Land Survey Office. https://ags.cuzk.cz/opendata/. Accessed 11 Mar 2024

[36] Dušánek P, Šíma J (2023) Ověření absolutní polohové přesnosti Ortofota ČR (2021 – 2022) [Verification of absolute positional accuracy - Orthophoto of the Czech Republic (2021 - 2022)]. Geodetický a kartografický obzor. Vol 69/111. Nr. 6.
[37] Metashape. Agisoft Metashape Professional Edition User Manual. https://www.agisoft.com/downloads/user-manuals/ Accessed 11 Mar 2024
[38] Luhmann T, Fraser C, Maas H-G (2016) Sensor modelling and camera calibration for close-range photogrammetry. ISPRS Journal of Photogrammetry and Remote Sensing 115:37–46. doi: 10.1016/j.isprsjprs.2015.10.006
[39] Pacina J, Popelka J, Tobisch M (2016) Extinct settlement identification using small format aerial photography – methods and accuracy. Advances and Trends in Engineering Sciences and Technologies II. doi: 10.1201/9781315393827-137
[40] Pacina J, Cajthaml J, Kratochvílová D, et al (2021) Pre-Dam Valley Reconstruction based on archival spatial data sources: Methods, accuracy, and 3D printing possibilities. Transactions in GIS 26:385–420. doi: 10.1111/tgis.12854
[41] Rousseeuw PJ (1984) Least median of squares regression. Journal of the American Statistical Association 79:871. doi: 10.2307/2288718